

# Systematic shell-model analysis of $2\nu\beta\beta$ decay of $^{76}\text{Ge}$ and $^{96}\text{Zr}$ to the ground and excited states of $^{76}\text{Se}$ and $^{96}\text{Mo}$

Deepak Patel,<sup>1</sup> Praveen C. Srivastava,<sup>1,\*</sup> and Jouni Suhonen<sup>2,3</sup>

<sup>1</sup>*Department of Physics, Indian Institute of Technology Roorkee, Roorkee 247667, India*

<sup>2</sup>*University of Jyväskylä, Department of Physics,*

*P.O. Box 35 (YFL), FI-40014, University of Jyväskylä, Finland*

<sup>3</sup>*International Centre for Advanced Training and Research in Physics (CIFRA),*

*P.O. Box MG12, 077125 Bucharest-Măgurele, Romania*

(Dated: April 19, 2024)

In this work, we have studied the  $2\nu\beta\beta$  decay of  $^{76}\text{Ge}$  and  $^{96}\text{Zr}$  isotopes utilizing large-scale shell-model calculations. The GWBXG effective interaction has been employed in the calculation of  $2\nu\beta\beta$ -decay nuclear matrix elements (NMEs). We have tested the effective interaction by comparing the predicted spectroscopic properties, such as energy spectra and transition probabilities, with the available experimental data. The variation of cumulative NMEs with respect to the  $1^+$  state energies of the intermediate nucleus is also studied, corresponding to  $0_{g.s.}^+ \rightarrow 0_{g.s.}^+$ ,  $0_{g.s.}^+ \rightarrow 0_2^+$ , and  $0_{g.s.}^+ \rightarrow 2_1^+$  transitions between the parent and granddaughter nuclei. The extracted half-lives using the shell-model predicted NMEs show good agreement with the recent experimental data. The comparison of the shell-model predicted NMEs with previous NMEs available in the literature is discussed. Also, the computed branching ratios for the  $2\nu\beta\beta$  decay of  $^{76}\text{Ge}$  and both the  $2\nu\beta\beta$  and single- $\beta$  decay of  $^{96}\text{Zr}$  are reported.

PACS numbers: 21.60.Cs, 23.20.-g, 23.20.Lv, 27.60.+j

## I. INTRODUCTION

Double beta decay (DBD) is a rare second-order weak-interaction process wherein a nucleus undergoes a simultaneous conversion of two neutrons into two protons, or vice versa [1–6]. This phenomenon, first proposed by Goeppert-Mayer in 1935 as a nuclear disintegration [7], plays a significant role in nuclear and particle physics. DBD occurs primarily in isotopes where single beta decay is energetically forbidden or highly suppressed. This process can occur through two decay modes: two-neutrino double beta decay ( $2\nu\beta\beta$ ) and neutrino-less double beta decay ( $0\nu\beta\beta$ ). In the realm of double beta decay studies,  $2\nu\beta\beta$  decay offers a valuable assessment of the standard model. It also confirms the validity of the weak nuclear forces and the existence of neutrinos as weakly interacting particles. The double- $\beta$ -minus mode of this decay process, relevant for the present studies, can be written as:  $(A, Z) \rightarrow (A, Z+2) + 2e^- + 2\bar{\nu}_e$ . In previous years, the  $2\nu\beta\beta$ -decay process has been observed in different mass regions of the nuclear chart for several nuclei. The study of  $2\nu\beta\beta$  decay mode also provides natural background components in  $0\nu\beta\beta$  measurements [8, 9]. In the case of the  $0\nu\beta\beta$  decay process, which is not observed yet, neutrino emission does not occur, thus violating lepton-number conservation [10, 11]. Determination of the half-lives of  $2\nu\beta\beta$  and  $0\nu\beta\beta$  decaying nuclei imparts crucial details about the decay rates and lifetimes of nuclei involved in the nucleosynthesis phenomenon [12]. In the present study, we consider only the  $2\nu\beta\beta$  decay process.

Several experiments have been performed for the accurate half-life estimation of the  $2\nu\beta\beta$ -decaying nuclei by different groups in the last few decades. In the NEMO-3 experiment, Arnold *et al.* [13] measured the half-life for  $2\nu\beta\beta$  decay of  $^{48}\text{Ca}$  to the ground state (g.s.) of  $^{48}\text{Ti}$  as  $T_{1/2}^{2\nu} = [6.4_{-0.6}^{+0.7}(\text{stat})_{-0.9}^{+1.2}(\text{syst})] \times 10^{19}$  yr. Recently, Agostini *et al.* [3] extracted the half-life of  $^{76}\text{Ge}$  for  $2\nu\beta\beta$  decay to the g.s. of  $^{76}\text{Se}$  as  $(2.022 \pm 0.018_{\text{stat}} \pm 0.038_{\text{syst}}) \times 10^{21}$  yr from the GERMANIUM DETECTOR ARRAY (GERDA). From another NEMO-3 experiment, Arnold *et al.* [14] studied the  $2\nu\beta\beta$  decay in  $^{82}\text{Se}$  to the g.s. of  $^{82}\text{Kr}$ ; they have measured the half-life as  $[9.39 \pm 0.17(\text{stat}) \pm 0.58(\text{syst})] \times 10^{19}$  yr and extracted the corresponding nuclear matrix element  $|M_{2\nu}| = 0.0498 \pm 0.0016$  using the value  $g_A = 1.27$  for the weak axial coupling. In the  $A = 90$  mass region,  $^{96}\text{Zr}$  is a well-known candidate of  $2\nu\beta\beta$  decay. Using the NEMO-3 detector, the obtained half-life of  $^{96}\text{Zr}$  in  $2\nu\beta\beta$  decay to the g.s. of  $^{96}\text{Mo}$  is  $T_{1/2}^{2\nu} = [2.35 \pm 0.14(\text{stat}) \pm 0.16(\text{syst})] \times 10^{19}$  yr and the extracted NME using the above half-life and  $g_A = 1.25$  is  $M_{2\nu} = 0.049 \pm 0.002$  [15]. Another candidate of  $2\nu\beta\beta$  decay,  $^{100}\text{Mo}$  has one of the largest decay energies,  $Q_{\beta\beta} = 3034.36(17)$  keV [16] and the shortest half-life [17]. Recently, Armengaud *et al.* [18] determined the g.s.-to-g.s. decay half-life of  $^{100}\text{Mo}$  very precisely as  $T_{1/2}^{2\nu} = [7.12_{-0.14}^{+0.18}(\text{stat}) \pm (\text{syst})] \times 10^{18}$  yr using the CUPID-Mo detection technology. In the Aurora experiment, the half-life of the  $2\nu\beta\beta$  transition of  $^{116}\text{Cd}$  to the  $0_{g.s.}^+$  of  $^{116}\text{Sn}$  was measured with the highest accuracy as  $T_{1/2}^{2\nu} = (2.63_{-0.12}^{+0.11}) \times 10^{19}$  yr [19]. In another work, the half-lives of two other  $2\nu\beta\beta$  decaying candidates,  $^{128,130}\text{Te}$ , were proposed as  $(2.41 \pm 0.39) \times 10^{24}$  and  $(9.0 \pm 1.4) \times 10^{20}$  yr, respectively, using geological Te specimens [20]. In the NEXT Collaboration,

\* Corresponding author: praveen.srivastava@ph.iitr.ac.in

Novella *et al.* [21] extracted the  $2\nu\beta\beta$  half-life of  $^{136}\text{Xe}$  as  $2.34^{+0.80}_{-0.46}(\text{stat})^{+0.30}_{-0.17}(\text{syst}) \times 10^{21}$  yr for the g.s. transition. After the nucleus  $^{48}\text{Ca}$ ,  $^{150}\text{Nd}$  has the second largest  $Q_{\beta\beta}$  value (3371.38 keV [16]), making it an intriguing nucleus for studying both  $2\nu\beta\beta$  and  $0\nu\beta\beta$  decay. Recently, Arnold *et al.* [22] reported findings on the search for  $0\nu\beta\beta$  decay and measured the  $2\nu\beta\beta$  decay half-life of  $^{150}\text{Nd}$  as  $T_{1/2}^{2\nu} = [9.34 \pm 0.22(\text{stat})^{+0.62}_{-0.60}(\text{syst})] \times 10^{18}$  yr for the g.s.-to-g.s transition in the NEMO-3 Collaboration.

The cumulative nuclear matrix elements ( $M_{2\nu}$ ) for  $2\nu\beta\beta$  decay should show a significant contribution from the Gamow-Teller giant resonance (GTGR) region. Nuclear models like proton-neutron quasi-particle random-phase approximation (pnQRPA) take the GTGR region into account in a realistic way [23, 24]. However, for the nuclear shell model the high energy in the GTGR region remains a challenge and could only partly be described by two earlier shell-model calculations in the case of  $^{48}\text{Ca}$  [25, 26]. In the past, due to huge dimensions, it was difficult to perform large-scale shell-model calculations for  $2\nu\beta\beta$  decay studies in the medium to heavier mass region. At present, it is possible to perform shell-model calculations in extended valence spaces, including the relevant shell-model configurations, due to significant progress in configuration mixing using novel approaches and new advancements in the computational facilities. All this could help us describe the GTGR region realistically within the shell-model framework in the near future.

We have studied the  $2\nu\beta\beta$  decay in several nuclei in our previous work [27], excluding  $^{76}\text{Ge}$  and  $^{96}\text{Zr}$ . Now, motivated by the recent experimental data [3, 28, 29] on the  $2\nu\beta\beta$ -decaying nuclei  $^{76}\text{Ge}$  and  $^{96}\text{Zr}$ , we have performed large-scale shell-model calculations for studying the behavior of cumulative NMEs with respect to the  $1^+$  state energies in the intermediate nucleus and extracting the  $2\nu\beta\beta$  half-lives of these two nuclei (using Eqs. 1 and 2 below). The contributions of the  $1^+$  states of the intermediate nucleus have been included up to the saturation level of NMEs. The present work represents the most comprehensive set of shell-model results thus far for the various  $\beta$  and/or  $2\nu\beta\beta$  transitions in  $^{76}\text{Ge}$  and  $^{96}\text{Zr}$ .

This paper is organized as follows: Sec. II provides a concise introduction to the theoretical framework used in our calculations. Sec. III presents the outcomes of the shell-model analyses and discussion regarding the energy spectra, transition probabilities, NMEs, extracted half-lives, and branching ratios. Finally, we summarize our findings and draw conclusions in Sec. IV.

## II. THEORETICAL FRAMEWORK

### A. Half-life

We can express the half-life for the  $2\nu\beta\beta$  decay as follows

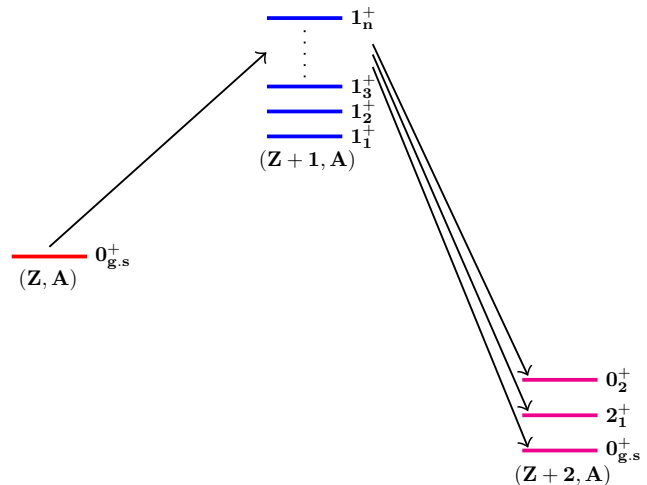


FIG. 1. Nuclear level and decay scheme for  $2\nu\beta\beta$ -minus decay.

$$(T_{1/2}^{2\nu})^{-1} = G^{2\nu} g_A^4 |M_{2\nu}|^2. \quad (1)$$

Here,  $G^{2\nu}$  denotes the phase-space factor [30–33] and  $g_A$  is the axial-vector coupling strength [34].  $M_{2\nu}$  is the nuclear matrix element (NME) for  $2\nu\beta\beta$  decay and first derived by Tomoda *et al.* [35]. We can express it by the following expression [36]

$$M_{2\nu} = \sum_N \frac{\langle J^+ || \sigma \tau^\pm || 1_N^+ \rangle \langle 1_N^+ || \sigma \tau^\pm || 0_{\text{g.s.}}^{(i)} \rangle}{\sqrt{J+1} ([\frac{1}{2} Q_{\beta\beta} + E(1_N^+) - M_i] / m_e + 1)^k}, \quad (2)$$

where  $m_e$  represents the rest mass of the electron;  $E(1_N^+) - M_i$  corresponds to the energy difference between the  $N^{\text{th}}$  intermediate  $1^+$  state and the ground state (g.s.) of the initial nucleus;  $0_{\text{g.s.}}^{(i)}$  stands for the ground state of the initial nucleus;  $\sigma$  is the Pauli spin operator;  $\tau^-$  ( $\tau^+$ ) is the isospin lowering (raising) operator.  $Q_{\beta\beta}$  ( $Q$ -value) is the energy released in the decay.  $\langle J^+ || \sigma \tau^\pm || 1_N^+ \rangle$  and  $\langle 1_N^+ || \sigma \tau^\pm || 0_{\text{g.s.}}^{(i)} \rangle$  denote the reduced Gamow-Teller (GT) matrix elements and  $J$  represents the spin state of the final nucleus. Here,  $k = 1$  for  $J = 0$  and  $k = 3$  for  $J = 2$  [37]. The nuclear energy and decay scheme for  $2\nu\beta\beta$ -minus decay is shown in Fig. 1.

### B. Shell-model Hamiltonian

We can express the nuclear shell-model Hamiltonian in terms of single-particle energies and two-nucleon interactions as [38]

$$H = T + V = \sum_{\alpha} \epsilon_{\alpha} \hat{N}_{\alpha} + \sum_{\alpha \leq \beta, \gamma \leq \delta, J, M} \langle j_{\alpha} j_{\beta} | V | j_{\gamma} j_{\delta} \rangle_J \times O_{\alpha, \beta}^{\dagger}(JM) O_{\gamma, \delta}(JM), \quad (3)$$

where  $\alpha = \{nljt\}$  stand for the single-particle orbitals with  $n$  being the number of nodes of the wave function,  $l$  the orbital angular momentum,  $j$  the total angular momentum, and  $t = 1/2$  the isospin. The  $\epsilon_{\alpha}$  represent the corresponding single-particle energies.  $\hat{N}_{\alpha} = \sum_{m_{\alpha}} c_{\alpha, m_{\alpha}}^{\dagger} c_{\alpha, m_{\alpha}}$  denotes the particle-number operator. The symbol  $\langle j_{\alpha} j_{\beta} | V | j_{\gamma} j_{\delta} \rangle_J$  is the two-body interaction matrix element.  $O_{\alpha, \beta}^{\dagger}(JM) (O_{\gamma, \delta}(JM))$  corresponds to the fermion pair creation (annihilation) operator and is written as

$$O_{\alpha, \beta}^{\dagger}(JM) = \frac{1}{\sqrt{1 + \delta_{\alpha\beta}}} \sum_{m_{\alpha}, m_{\beta}} \langle j_{\alpha} m_{\alpha} j_{\beta} m_{\beta} | JM \rangle \times c_{\alpha, m_{\alpha}}^{\dagger} c_{\beta, m_{\beta}}^{\dagger}. \quad (4)$$

We have employed the GWBXXG effective shell-model Hamiltonian in our calculations, where its mean-field part consists of the  $0f_{5/2}$ ,  $1p_{3/2}$ ,  $1p_{1/2}$ , and  $0g_{9/2}$  proton orbitals, as well as  $1p_{1/2}$ ,  $0g_{9/2}$ ,  $0g_{7/2}$ ,  $1d_{5/2}$ ,  $1d_{3/2}$ , and  $2s_{1/2}$  neutron orbitals. This interaction is a composition of different interactions. The initial 974 two-body matrix elements (TBMEs) are derived from the bare  $G$ -matrix of the H7B potential [39]. The bare  $G$ -matrix is not reasonable due to the space truncation, and the interaction should be renormalized by considering the core-polarization effects. Here, the present  $G$ -matrix effective interaction is tuned by further modification in matrix elements using fitted interactions: The 65 TBMEs for proton orbitals are replaced with the effective values reported in Ref. [40]. The TBMEs connecting the  $\pi(1p_{1/2}, 0g_{9/2})$  and the  $\nu(1d_{5/2}, 2s_{1/2})$  orbitals are replaced by those from the Ref. [41]. Further, Serduke *et al.* [42] replaced the TBMEs between the  $\pi(1p_{1/2}, 0g_{9/2})$  and the  $\nu(1p_{1/2}, 0g_{9/2})$  orbitals.

It is difficult to calculate all possible  $1^+$  states of intermediate nuclei in the full model space due to the involved huge dimensions. Thus, we have employed truncation on neutron orbitals above  $N = 50$  for calculating the  $2\nu\beta\beta$ -decay NME in  $^{76}\text{Ge}$ . Here, we have performed  $1p - 1h$  excitation across  $N = 50$  to the  $0g_{7/2}$ ,  $1d_{5/2}$ ,  $1d_{3/2}$ , and  $2s_{1/2}$  neutron orbitals. For the calculation of the  $2\nu\beta\beta$ -decay NME in  $^{96}\text{Zr}$ , we have applied the truncation, where the considered proton and neutron partitions belong to the  $\pi[(0f_{5/2}1p_{3/2})^{0-10}(1p_{1/2}0g_{9/2})^{0-4}]$  and  $\nu[(1p_{1/2}0g_{9/2})^{12-12}(0g_{7/2}1d_{5/2}1d_{3/2}2s_{1/2})^{0-20}]$  configurations, respectively. In both calculations, we have considered 5000 eigenvalues for  $1^+$  states in  $^{76}\text{As}$  and  $^{96}\text{Nb}$ . The shell-model codes NuShellX [43] and KShell [44] have been used in the diagonalization of the shell-model Hamiltonian matrices.

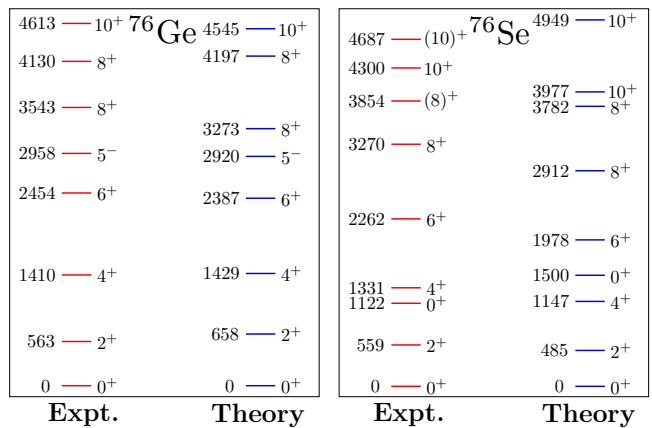


FIG. 2. Comparison between experimental and shell-model calculated low-lying states in  $^{76}\text{Ge}$  and  $^{76}\text{Se}$ .

### III. RESULTS AND DISCUSSION

In this section, we present the results obtained from shell-model calculations. First, we discuss the theoretical and experimental energy spectra and the corresponding quadrupole-reduced transition probabilities ( $B(E2)$ ) for the parent, and granddaughter nuclei of interest in the  $2\nu\beta\beta$ -decay study. We also show the variation of the shell-model calculated cumulative NME as a function of the excitation energy of the  $1^+$  states of the intermediate nucleus. Using the final predicted NMEs, we extract the  $2\nu\beta\beta$ -decay half-lives of  $^{76}\text{Ge}$  and  $^{96}\text{Zr}$ . We also compare our calculated NMEs with the previously available NMEs in the literature. Lastly, we estimate the branching ratios for the  $2\nu\beta\beta$  decay of  $^{76}\text{Ge}$  and for both the single- $\beta$  and  $2\nu\beta\beta$  decay modes of  $^{96}\text{Zr}$ .

#### A. Energy spectra and electromagnetic properties

In Fig. 2, we depict the comparison between the shell-model and experimental low-energy states of the  $^{76}\text{Ge}$  and  $^{76}\text{Se}$  isotopes. It is clear from the spectra that our calculated states are in quite good agreement with the experimental data for both isotopes. In  $^{76}\text{Ge}$ , the shell-model predicted positive-parity yrast states (g.s. band) up to  $8_1^+$  are characterized by mainly  $[\pi(f_{5/2}^4) \otimes \nu(g_{9/2}^6)]$  configuration, whereas the  $10_1^+$  state stems from  $[\pi(f_{5/2}^2 p_{3/2}^2) \otimes \nu(g_{9/2}^6) \approx 25.3\%]$  and  $[\pi(f_{5/2}^4) \otimes \nu(g_{9/2}^6) \approx 21.8\%]$  configurations. Here, the large energy gap between the  $8_1^+$  and  $10_1^+$  states compared to the other two consecutive yrast states may be caused by the excitation of two protons from the  $\pi(f_{5/2})$  orbital to the  $\pi(p_{3/2})$  orbital in the dominant configuration of the  $10_1^+$  state. Contrariwise, the yrast  $0_{g.s.}^+ - 10_1^+$  states (g.s. band) in  $^{76}\text{Se}$  are described by same dominant configuration  $\pi(f_{5/2}^2 p_{3/2}^2 g_{9/2}^2) \otimes \nu(g_{9/2}^4)$ . The excited states in the yrast band of  $^{76}\text{Ge}$  and  $^{76}\text{Se}$  show a pronounced collective be-

TABLE I. Comparison of theoretical and experimental  $B(E2)$  strengths (in  $e^2\text{fm}^4$ ) [45] in the parent and grand-daughter nuclei of  $2\nu\beta\beta$  decay. The effective charges are taken as  $e_\pi = 1.6e$ ,  $e_\nu = 0.8e$  [46].

Isotope	$J_i^\pi \rightarrow J_f^\pi$	Theory	Expt.
$^{76}\text{Ge}$	$2_1^+ \rightarrow 0_1^+$	330.7	554.5(191)
	$4_1^+ \rightarrow 2_1^+$	435.4	726.6(1721)
$^{76}\text{Se}$	$2_1^+ \rightarrow 0_1^+$	553.3	841.4(191)
	$4_1^+ \rightarrow 2_1^+$	811.3	1357.7(382)
	$6_1^+ \rightarrow 4_1^+$	921.9	1300.3(1530)
	$8_1^+ \rightarrow 6_1^+$	961.4	1568.0(3251)
	$10_1^+ \rightarrow 8_1^+$	1031.2	994.4(2103)
$^{96}\text{Zr}$	$2_1^+ \rightarrow 0_1^+$	62.2	60.1(78)
	$3_1^+ \rightarrow 2_1^+$	0.1	2.6(+78-26)
	$8_1^+ \rightarrow 6_4^+$	39.6	36.0(29)
$^{96}\text{Mo}$	$2_1^+ \rightarrow 0_1^+$	266.6	540.5(104)
	$4_1^+ \rightarrow 2_1^+$	307.6	1070.5(1828)
	$3_1^+ \rightarrow 2_1^+$	1.0	< 33.9
	$6_1^+ \rightarrow 4_1^+$	243.8	< $75.7 \times 10^2$

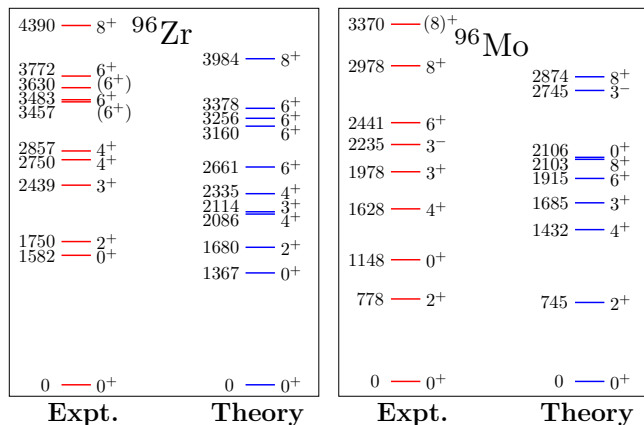


FIG. 3. Comparison between experimental and shell-model calculated low-lying states in  $^{96}\text{Zr}$  and  $^{96}\text{Mo}$ .

havior. The experimental data for  $B(E2)$  transitions in the yrast band of  $^{76}\text{Ge}$  are available only for  $2_1^+ - 0_1^+$  and  $4_1^+ - 2_1^+$  transitions. As reported in Table I, except for the  $10_1^+ - 8_1^+$  transition in  $^{76}\text{Se}$ , our calculated  $B(E2)$  transitions for both isotopes are slightly smaller but consistent with the experimental data.

Fig. 3 shows a comparison between the shell-model predicted and the experimental low-lying energy states in  $^{96}\text{Zr}$  and  $^{96}\text{Mo}$ . The  $0_{\text{g.s.}}^+$  in  $^{96}\text{Zr}$  arises primarily due to the pure  $\pi(g_{9/2}^2) \otimes \nu(d_{5/2}^6)$  configuration, whereas the  $0_2^+$  and  $2_1^+$  states stem from the proton-aligned configuration  $\pi(g_{9/2}^2)$  and the collective contribution  $\nu(d_{5/2}^4 g_{7/2}^2)$  of neutron orbitals, although the wavefunctions of both states are quite fragmented. Experimentally, the nucleus  $^{96}\text{Zr}$

exhibits a small  $B(E2; 2_1^+ \rightarrow 0_1^+)$  transition strength, verifying the similar value obtained in our calculation. Structure change between the involved initial and final states may cause this small  $B(E2)$  value. Similarly, we obtain different structures in the largest configuration of the  $8_1^+$  and  $6_4^+$  states, namely  $[\pi(g_{9/2}^2) \otimes \nu(g_{7/2}^2 d_{5/2}^4)]$  and  $[\pi(p_{1/2}^2) \otimes \nu(g_{7/2}^1 d_{5/2}^5)]$ , due to which we record a small  $B(E2; 8_1^+ \rightarrow 6_4^+)$  value, similar to the experimental one (see Table I). In the case of  $^{96}\text{Mo}$ , the g.s. sequence  $0_1^+ - 8_1^+$  shows similar structure with the dominant configuration  $\pi(g_{9/2}^2) \otimes \nu(d_{5/2}^4)$  predicted by the shell model. Thus, as reported in Table I, the obtained  $B(E2)$  values are not weak for the  $2_1^+ \rightarrow 0_1^+$ ,  $4_1^+ \rightarrow 2_1^+$ , and  $6_1^+ \rightarrow 4_1^+$  transitions but still they are not even half of the experimental values. The choice of effective charges might be a reason for relatively smaller  $B(E2)$  values, but this is outside the scope of the present study. However, overall, the computed  $B(E2)$  values of Table I are in quite a good agreement with the experimental data.

After analyzing these results for energy spectra and transition probabilities, we are confident that the present shell-model Hamiltonian can be safely employed in calculating the NMEs ( $M_{2\nu}$ ) for our  $2\nu\beta\beta$ -decay study.

## B. Cumulative nuclear matrix elements and the extracted half-lives

Here, we discuss the shell-model calculated results for NMEs and half-lives for the  $2\nu\beta\beta$  decays of  $^{76}\text{Ge}$  and  $^{96}\text{Zr}$ . The calculated NMEs and half-lives are reported in Table II. We have taken the  $Q_{\beta\beta}$  and  $Q_\beta$  values from Ref. [16]. In the case of  $0_{\text{g.s.}}^+ \rightarrow 0_2^+$  and  $0_{\text{g.s.}}^+ \rightarrow 2_1^+$  transitions, the  $Q_{\beta\beta}$  values are taken as the difference of the  $Q_\beta$  value and the experimental energies of  $0_2^+$  and  $2_1^+$  states, respectively. The variation of cumulative NMEs as a function of  $1^+$  state energies of the intermediate nucleus is depicted in Figs. 4-5.

**$^{76}\text{Ge}$ :** A careful and precise calculation of NMEs ( $M_{2\nu}$ ) holds significant importance in the theoretical analysis of the  $2\nu\beta\beta$  decay of a nucleus. In the case of  $^{76}\text{Ge}$ , we have calculated  $M_{2\nu}$  for three transitions:  $0_{\text{g.s.}}^+ \rightarrow 0_{\text{g.s.}}^+$ ,  $0_{\text{g.s.}}^+ \rightarrow 0_2^+$ , and  $0_{\text{g.s.}}^+ \rightarrow 2_1^+$ . In the present calculation, the excitation energies of  $1^+$  states in  $^{76}\text{As}$  were shifted such that the lowest-lying  $1^+$  state is at the experimental energy of 0.044 MeV. As reported in Table III, the first  $1^+$  state of the intermediate nucleus contributes 55.8% of the final NME (0.2285), yielding a value of 0.1275 for the  $0_{\text{g.s.}}^+ \rightarrow 0_{\text{g.s.}}^+$  transition. In this case, we can see from Fig. 4 that the cumulative NME peaks around 4.35 MeV, with a value of 0.2671. As mentioned earlier, the pnQRPA calculations realistically incorporate the contribution of the GTGR region to the NMEs [23, 24]. But, to the best of our knowledge, previous shell-model calculations were able to describe this region partly in the case of only  $^{48}\text{Ca}$  [25, 26]. In our case for the  $0_{\text{g.s.}}^+ \rightarrow 0_{\text{g.s.}}^+$  transition, the peak is found at the



TABLE II. Shell-model calculated  $2\nu\beta\beta$  NMEs and the extracted half-lives. The phase-space factors ( $G^{2\nu}$ ) are taken from Ref. [30].

Transition	$ M_{2\nu} $	$G^{2\nu}$ (yr $^{-1}$ )	$g_A^{\text{eff}}$	Calculated $T_{1/2}^{2\nu}$ (yr)	Experimental/Recommended value of $T_{1/2}^{2\nu}$ (yr)
$^{76}\text{Ge}(0_{\text{g.s.}}^+) \rightarrow ^{76}\text{Se}(0_{\text{g.s.}}^+)$	0.2285	$4.51 \times 10^{-20}$	0.80	$1.037 \times 10^{21}$	$(2.022 \pm 0.018_{\text{stat}} \pm 0.038_{\text{syst}}) \times 10^{21}$ [3]
$^{76}\text{Ge}(0_{\text{g.s.}}^+) \rightarrow ^{76}\text{Se}(0_2^+)$	0.2414	$6.4 \times 10^{-23}$		$6.546 \times 10^{23}$	$> 6.2 \times 10^{21}$ [47]
$^{76}\text{Ge}(0_{\text{g.s.}}^+) \rightarrow ^{76}\text{Se}(2_1^+)$	0.0045	$4.0 \times 10^{-22}$		$3.014 \times 10^{26}$	$> 1.1 \times 10^{21}$ [48]
$^{96}\text{Zr}(0_{\text{g.s.}}^+) \rightarrow ^{96}\text{Mo}(0_{\text{g.s.}}^+)$	0.0599	$642.0 \times 10^{-20}$	1.00	$4.341 \times 10^{19}$	$(2.35 \pm 0.14(\text{stat}) \pm 0.16(\text{syst})) \times 10^{19}$ [15]
$^{96}\text{Zr}(0_{\text{g.s.}}^+) \rightarrow ^{96}\text{Mo}(0_2^+)$	0.0159	$1633.8 \times 10^{-22}$		$2.421 \times 10^{22}$	$> 3.1 \times 10^{20}$ [28]
$^{96}\text{Zr}(0_{\text{g.s.}}^+) \rightarrow ^{96}\text{Mo}(2_1^+)$	$7.4 \times 10^{-4}$	$730.8 \times 10^{-21}$		$2.499 \times 10^{24}$	$> 4.1 \times 10^{19}$ [49]

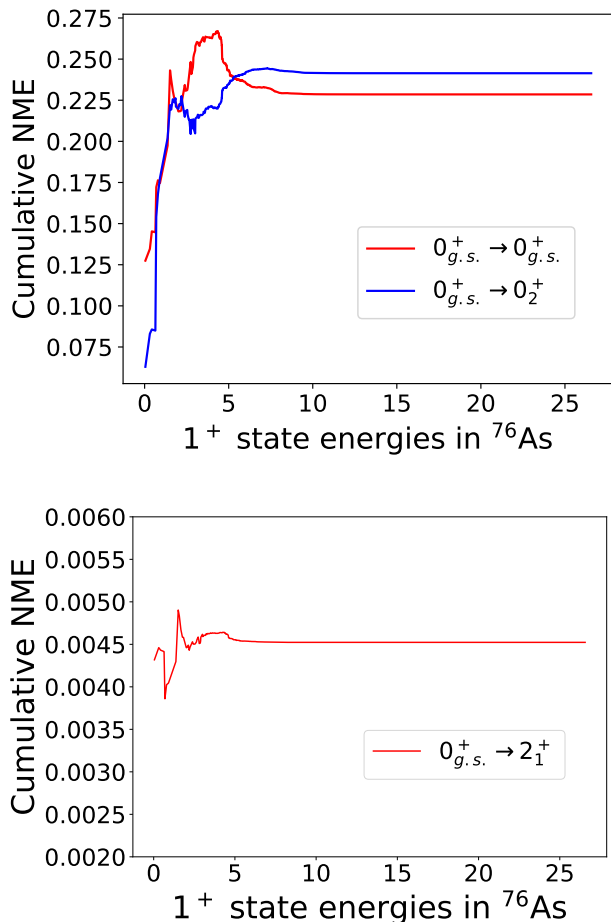


FIG. 4. Cumulative  $2\nu\beta\beta$  NMEs ( $M_{2\nu}$ ) for  $^{76}\text{Ge}$  as functions of excitation energy of the intermediate  $1^+$  state in  $^{76}\text{As}$ .

$85^{\text{th}}$  intermediate  $1^+$  state; however, this energy (4.35 MeV) is notably below the energy of the GT resonance ( $\approx 11$  MeV) [50]. Comparison of our results with those of the large-scale shell-model calculations of Kostensalo *et al.* [36] shows that the calculation of [36] does not show a prominent peak at this energy, and only a small

TABLE III. Contribution in the final NME from the first  $1^+$  state of the intermediate nucleus.

Transitions	Value	Percentage (%)
$^{76}\text{Ge}(0_{\text{g.s.}}^+) \rightarrow ^{76}\text{Se}(0_{\text{g.s.}}^+)$	0.1275	55.8
$^{76}\text{Ge}(0_{\text{g.s.}}^+) \rightarrow ^{76}\text{Se}(0_2^+)$	0.0630	26.1
$^{76}\text{Ge}(0_{\text{g.s.}}^+) \rightarrow ^{76}\text{Se}(2_1^+)$	0.0043	95.6
$^{96}\text{Zr}(0_{\text{g.s.}}^+) \rightarrow ^{96}\text{Mo}(0_{\text{g.s.}}^+)$	0.0596	99.5
$^{96}\text{Zr}(0_{\text{g.s.}}^+) \rightarrow ^{96}\text{Mo}(0_2^+)$	0.0032	20.1

bump at around 5 MeV of excitation can be discerned. After around 12.75 MeV, the cumulative NMEs for the  $0_{\text{g.s.}}^+ \rightarrow 0_{\text{g.s.}}^+$  transition start to saturate and show almost constant behavior with a final value of 0.2285. Similarly, for the  $0_{\text{g.s.}}^+ \rightarrow 0_2^+$  and  $0_{\text{g.s.}}^+ \rightarrow 2_1^+$  transitions, the cumulative NMEs nearly saturate after around 11.69 and 7.55 MeV with the final values 0.2414 and 0.0045, respectively. Using Eq. (1) and utilizing the final value of NME (0.2285) for the  $0_{\text{g.s.}}^+ \rightarrow 0_{\text{g.s.}}^+$  transition, together with  $g_A^{\text{eff}} = 0.8$  [34], we have extracted the half-life of  $^{76}\text{Ge}$  as  $1.037 \times 10^{21}$  yr, which shows good agreement with the experimental half-life [3] (see Table II). In the case of  $0_{\text{g.s.}}^+ \rightarrow 0_2^+$ , and  $0_{\text{g.s.}}^+ \rightarrow 2_1^+$  transitions, the cumulative NMEs show a very similar behavior as recorded in the shell-model calculation of [36]. The corresponding calculated half-lives are  $6.546 \times 10^{23}$  and  $3.014 \times 10^{26}$  yr, respectively. Both estimates are notably higher than the experimental lower limits  $6.2 \times 10^{21}$  [47] and  $1.1 \times 10^{21}$  yr [48]. These results may be useful for experimentalists in estimating the sensitivities of their experimental set-ups to these  $0_{\text{g.s.}}^+ \rightarrow 0_2^+$ , and  $0_{\text{g.s.}}^+ \rightarrow 2_1^+$  transitions in the future.

**$^{96}\text{Zr}$ :** Because of the large  $Q$ -value (3356.03 keV),  $^{96}\text{Mo}$  has several excited states through which  $^{96}\text{Zr}$  could undergo  $2\nu\beta\beta$  decay. Here, we have taken three transitions  $0_{\text{g.s.}}^+ \rightarrow 0_{\text{g.s.}}^+$ ,  $0_{\text{g.s.}}^+ \rightarrow 0_2^+$ , and  $0_{\text{g.s.}}^+ \rightarrow 2_1^+$  from the parent to granddaughter nucleus for calculating the  $M_{2\nu}$  and extracting the  $2\nu\beta\beta$ -decay half-lives, like in the case of  $^{76}\text{Ge}$ . There is no  $1^+$  state having been experimentally confirmed for  $^{96}\text{Nb}$ . Thus, shell-model computed

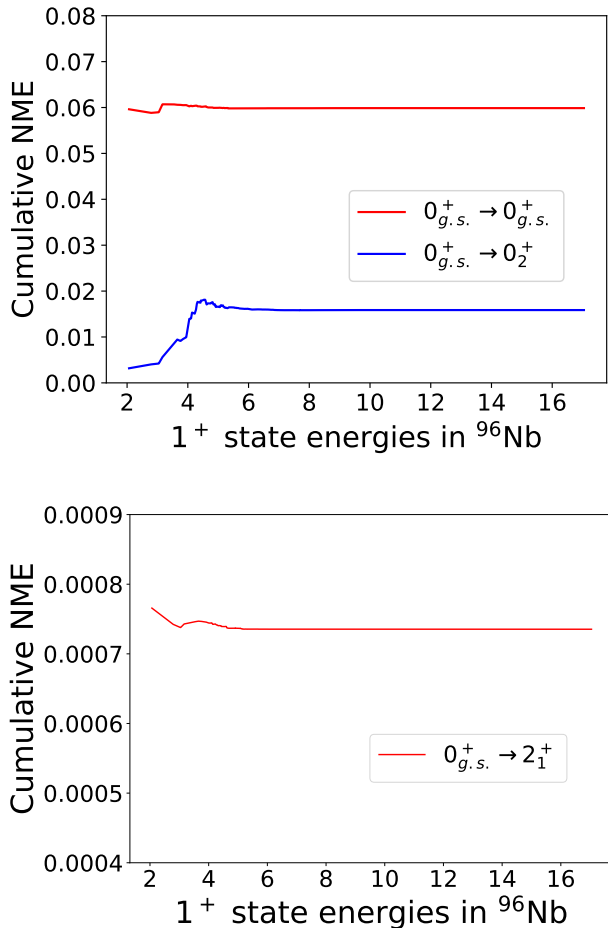


FIG. 5. Cumulative  $2\nu\beta\beta$  NMEs ( $M_{2\nu}$ ) for  $^{96}\text{Zr}$  as functions of excitation energy of the intermediate  $1^+$  state in  $^{96}\text{Nb}$ .

excitation energies are used to calculate the NMEs. In our calculation, we found that the contribution in the cumulative NME from the first  $1^+$  state of the intermediate nucleus for the  $0_{g.s.}^+ \rightarrow 0_{g.s.}^+$  transition is 0.0596, accounting for 99.5% of the final value (0.0599). Thus, it demonstrates a clear single-state dominance (SSD), consistent with the previous study [25]. On the contrary, the  $1_1^+$  state of  $^{96}\text{Nb}$  contributes 20.1% to the final NME (0.0159) for the  $0_{g.s.}^+ \rightarrow 0_2^+$  transition. Interestingly, the  $0_{g.s.}^+ \rightarrow 2_1^+$  transition exhibits SSD with a value 0.00077 of the cumulative NME, which is slightly higher than the final NME (0.00074). Therefore, we have not reported its contributive percentage in Table III.

The extracted half-lives of  $^{96}\text{Zr}$  using the final NMEs for the  $0_{g.s.}^+ \rightarrow 0_{g.s.}^+$ ,  $0_{g.s.}^+ \rightarrow 0_2^+$ , and  $0_{g.s.}^+ \rightarrow 2_1^+$  transitions are  $4.341 \times 10^{19}$ ,  $2.421 \times 10^{22}$ , and  $2.499 \times 10^{24}$  yr, respectively. Here, we have taken  $g_A^{\text{eff}} = 1.00$  [51]. However, utilizing  $g_A^{\text{eff}} = 1.04$  as proposed in Ref. [25], we would obtain a half-life for the  $0_{g.s.}^+ \rightarrow 0_{g.s.}^+$  transition slightly closer to the experimental value. The computed half-lives for the  $0_{g.s.}^+ \rightarrow 0_2^+$  and  $0_{g.s.}^+ \rightarrow 2_1^+$  transitions

are notably higher than the lower limit of experimental values, which could be useful in estimating experimental sensitivities to these transitions in the future.

### C. Comparison of NMEs

Here, we discuss the comparison between our shell-model predicted and earlier suggested NMEs using different nuclear models, as reported in Table IV. We notice that the previously determined NMEs for  $^{76}\text{Ge}$  exhibit either a notably small value (0.034) [52] or significantly large value (0.879) [53] with respect to correctly reproducing the experimental half-life for the  $0_{g.s.}^+ \rightarrow 0_{g.s.}^+$  transition. The NME (0.168) obtained in Ref. [36] is approximately 1.36 times smaller than our calculated NME, and the one of [54] (0.074) is about half of the one of [36]. We have allowed  $1p-1h$  excitations across the neutron-shell closure  $N = 50$ , which is not considered in the previous study [36]. It is a possible cause for the relatively larger value of the NME in our case. We have accounted for the contribution of a huge number of excited  $1^+$  states in the intermediate nucleus  $^{76}\text{As}$ , hence, it is reasonable to involve also the contribution of those  $1^+$  states which are arising due to the  $1p-1h$  excitations across the  $N = 50$  shell gap. Notably, the final NME for the  $0_{g.s.}^+ \rightarrow 0_2^+$  transition is larger than for the ground-state transition. Similar results concerning the calculated NMEs for the  $0_{g.s.}^+ \rightarrow 0_{g.s.}^+$  and  $0_{g.s.}^+ \rightarrow 0_2^+$  transitions were also found in previous studies, utilizing the interacting boson model (IBM) [52] and the renormalized quasiparticle random-phase approximation (RQRPA) [54] for  $^{76}\text{Ge}$ , as also the quasiparticle random-phase approximation (QRPA) [55] for  $^{136}\text{Xe}$ .

Previously, Šimkovic *et al.* [56] proposed that the NME for the  $0_{g.s.}^+ \rightarrow 0_{g.s.}^+$  transition in  $2\nu\beta\beta$  decay of  $^{76}\text{Ge}$  is suppressed because of the different deformations of the parent and granddaughter nucleus. We can deduce the deformation parameter ( $\beta_2$ ) from the intrinsic quadrupole moment ( $Q_0$ ). The  $\beta_2$  value is related to the  $Q_0$ -moment by the following expression [57]

$$\beta_2 = \frac{\sqrt{5\pi}}{3ZR^2} Q_0. \quad (5)$$

Here, for simplicity, we have taken  $R$  as  $1.2 \times A^{1/3}$  fm. Initially, we determined the  $Q_0$ -moment using the spectroscopic quadrupole moment,  $Q_s(2_1^+) = -28.714$  efm<sup>2</sup> in  $^{76}\text{Ge}$  obtained from our shell-model calculation, employing the formula  $Q_0 = -(7/2)Q_s$  [56] which arises from the expression [57]

$$Q_s = \frac{3K^2 - I(I+1)}{(I+1)(2I+3)} Q_0, \quad (6)$$

by taking  $K = 0$  for  $I^\pi = 2^+$ . Substituting the  $Q_0$  value into Eq. (5), we find the  $\beta_2$  value to be approximately 0.161. Similarly, utilizing the calculated  $Q_s(2_1^+)$

TABLE IV. Comparison between our calculated and previously obtained absolute values of NMEs. Here SM denotes the nuclear shell model, IBM the interacting boson model, HFB the Hartree-Fock-Bogoliubov theory, and (R)QRPA the (renormalized) quasiparticle random-phase approximation. For more values of NMEs of older calculations, see [60].

Transitions	NME					
	Present work	SM [36]	IBM [52]	HFB [53]	RQRPA [54]	QRPA [59]
$^{76}\text{Ge}(0_{\text{g.s.}}^+) \rightarrow ^{76}\text{Se}(0_{\text{g.s.}}^+)$	0.2285	0.168	0.034	0.879	0.074	-
$^{76}\text{Ge}(0_{\text{g.s.}}^+) \rightarrow ^{76}\text{Se}(0_2^+)$	0.2414	0.121	0.078	-	0.130	-
$^{76}\text{Ge}(0_{\text{g.s.}}^+) \rightarrow ^{76}\text{Se}(2_1^+)$	0.0045	0.0012	-	1.04	0.003	-
$^{96}\text{Zr}(0_{\text{g.s.}}^+) \rightarrow ^{96}\text{Mo}(0_{\text{g.s.}}^+)$	0.0599	-	0.154	-	0.036	0.022
$^{96}\text{Zr}(0_{\text{g.s.}}^+) \rightarrow ^{96}\text{Mo}(0_2^+)$	0.0159	-	0.063	-	0.028	0.012
$^{96}\text{Zr}(0_{\text{g.s.}}^+) \rightarrow ^{96}\text{Mo}(2_1^+)$	$7.4 \times 10^{-4}$	-	-	-	0.010	$8.1 \times 10^{-5}$

value (37.142 fm<sup>2</sup>) for  $^{76}\text{Se}$  from our shell-model calculation, we obtain the value  $\beta_2 = -0.195$ . Previous  $\beta_2$  values computed for  $^{76}\text{Ge}$  (0.157) and  $^{76}\text{Se}$  (-0.244) within relativistic mean field (RMF) theory [58] also support our findings. As suggested in Ref. [56], the behavior of final NME can be predicted by the value  $\Delta\beta_2 = |\beta_2(^{76}\text{Ge}) - \beta_2(^{76}\text{Se})|$  and the suppression of the  $2\nu\beta\beta$ -decay NME becomes stronger with an increase of  $\Delta\beta_2$ . Different deformation (prolate for  $^{76}\text{Ge}$  and oblate for  $^{76}\text{Se}$ ) yields a larger  $\Delta\beta_2$ , which may be a possible factor for the suppression of the NME for the  $0_{\text{g.s.}}^+ \rightarrow 0_{\text{g.s.}}^+$  transition in our case (see Fig. 4).

In the case of  $^{96}\text{Zr}$ , our computed value of the NME, 0.0599, for the  $0_{\text{g.s.}}^+ \rightarrow 0_{\text{g.s.}}^+$  transition, is slightly smaller than the 0.0747 one of [25]. Looking at Table IV, the previously determined NME using the IBM is larger than those obtained in the other theory frameworks. In fact, the present shell-model results for this transition are in good agreement with the RQRPA results of Toivanen *et al.* [54] and QRPA results of Stoica [59]. For the  $0_{\text{g.s.}}^+ \rightarrow 0_2^+$  transition a similar situation prevails, the IBM result deviating notably from the rest. Concerning the  $0_{\text{g.s.}}^+ \rightarrow 2_1^+$  transition, the RQRPA [54] gives a much larger NME than the present calculation and the QRPA model of Stoica [59]. Our NME for the  $0_{\text{g.s.}}^+ \rightarrow 2_1^+$  transition agrees qualitatively with the one of [59] although is one order of magnitude larger than it. Here it has to be pointed out that we have completely blocked neutron excitations across the  $N = 50$  shell closure in order to make the calculation of the NMEs for  $^{96}\text{Zr}$  feasible. Further, restricting the occupancy of the  $\pi(0g_{9/2})$  orbital to a maximum of four protons may cause inaccuracies in predicting the wave functions of the states of interest. In the future, one could achieve more precise NMEs if it was possible to include additional proton excitations in  $\pi(0g_{9/2})$  orbital and the contribution of the  $\nu(1p_{1/2})$  and  $\nu(0g_{9/2})$  orbitals.

#### D. Branching ratios

The nucleus  $^{76}\text{Ge}$  can decay via  $2\nu\beta\beta$  decay into the g.s. and different excited states of  $^{76}\text{Se}$ . But, the nucleus

$^{96}\text{Zr}$  can decay via  $2\nu\beta\beta$  decay into the g.s. and different excited states of  $^{96}\text{Mo}$  and also it can decay via single- $\beta$  transitions into the lowest  $4^+$ ,  $5^+$ , and  $6^+$  states of  $^{96}\text{Nb}$ . Here, we discuss the shell-model predicted branching ratios for the  $2\nu\beta\beta$  and/or single- $\beta$  transitions for the  $^{76}\text{Ge}$  and  $^{96}\text{Zr}$  decays.

In the case of  $^{76}\text{Ge}$ , we first calculated the total half-life for the  $0_{\text{g.s.}}^+ \rightarrow 0_{\text{g.s.}}^+$ ,  $0_{\text{g.s.}}^+ \rightarrow 0_2^+$ , and  $0_{\text{g.s.}}^+ \rightarrow 2_1^+$  transitions of  $2\nu\beta\beta$  decay using the formula [61]

$$\frac{1}{T_{1/2}^{\text{total}}} = \sum_k \frac{1}{T_{1/2}^k}, \quad (7)$$

where  $k$  refers to the final state of the decay. Subsequently, we have calculated the branching ratios ( $B.R.$ ),  $(B.R.)^k = T_{1/2}^{\text{total}}/T_{1/2}^k$  [61] for all three transitions. It is clear from the computed  $B.R.$  that the  $0_{\text{g.s.}}^+ \rightarrow 0_{\text{g.s.}}^+$  transition is dominant having the largest  $B.R.$  of 99.84%. The  $B.R.$  is notably smaller for the  $0_{\text{g.s.}}^+ \rightarrow 0_2^+$  transition ( $15.81 \times 10^{-2}\%$ ), and negligible for the  $0_{\text{g.s.}}^+ \rightarrow 2_1^+$  transition ( $3.43 \times 10^{-4}\%$ ).

Our estimated half-lives for the fourth-forbidden non-unique, fourth-forbidden unique, and sixth-forbidden non-unique  $\beta$  transitions from the  $0_{\text{g.s.}}^+$  of  $^{96}\text{Zr}$  to the  $4_1^+$ ,  $5_1^+$ , and  $6_1^+$  states of  $^{96}\text{Nb}$  (corresponding to  $g_A = g_V = 1$ ) are  $7.5 \times 10^{22}$ ,  $1.4 \times 10^{20}$ , and  $1.9 \times 10^{29}$  yr, respectively. These are quite similar to the half-lives  $7.5 \times 10^{22}$ ,  $1.1 \times 10^{20}$ , and  $1.6 \times 10^{29}$  yr obtained in Ref. [62]. Our results predict that the  $2\nu\beta\beta$  decay branching ratio (76.33%) is larger than the  $\beta$  decay branching ratio (23.67%) in  $^{96}\text{Zr}$ , consistently with the earlier shell-model study [36] where the  $2\nu\beta\beta$  branching ratio was 81.6%. In the QRPA study of [63] the  $\beta$  decay was dominated by the  $0_{\text{g.s.}}^+ \rightarrow 5_1^+$  transition with a half-life of  $2.4 \times 10^{20}$  yr, in agreement with the present study. In the  $2\nu\beta\beta$  branch of  $^{96}\text{Zr}$ , the  $0_{\text{g.s.}}^+ \rightarrow 0_{\text{g.s.}}^+$  transition is dominant with a 76.19% contribution, while the contributions from  $0_{\text{g.s.}}^+ \rightarrow 0_2^+$  ( $13.66 \times 10^{-2}\%$ ), and  $0_{\text{g.s.}}^+ \rightarrow 2_1^+$  ( $1.32 \times 10^{-3}\%$ ) transitions are almost negligible. In the case of the single- $\beta$  branch, the  $0_{\text{g.s.}}^+ \rightarrow 5_1^+$  transition dominates with 23.63% contribution, consistently with the previous study [36]. We found signifi-

cantly smaller branching ratios for the  $0_{g.s.}^+ \rightarrow 4_1^+$  (0.04%) and  $0_{g.s.}^+ \rightarrow 6_1^+$  ( $0.17 \times 10^{-7}\%$ ) transitions, again consistently with the studies of Kostensalo *et al.* [36] and Heiskanen *et al.* [63].

#### IV. SUMMARY AND CONCLUSIONS

In the present study, we have investigated the  $2\nu\beta\beta$  decay in  $^{76}\text{Ge}$  and  $^{96}\text{Zr}$  isotopes by using the GWBXXG shell-model effective Hamiltonian. Firstly, we validated the applicability of this Hamiltonian by computing low-lying energy levels and reduced transition probabilities in both parent and granddaughter nuclei. Our findings indicate that the present shell-model interaction is suitable for calculating NMEs for  $2\nu\beta\beta$  decay. To ensure the convergence of cumulative NMEs, we computed 5000  $1^+$  states in  $^{76}\text{As}$  and  $^{96}\text{Nb}$ . Utilizing the calculated NMEs, we extracted the half-lives of  $^{76}\text{Ge}$  and  $^{96}\text{Zr}$  for the  $0_{g.s.}^+ \rightarrow 0_{g.s.}^+$ ,  $0_{g.s.}^+ \rightarrow 0_2^+$ , and  $0_{g.s.}^+ \rightarrow 2_1^+$  transitions through  $2\nu\beta\beta$  decay. We further investigated the variation of cumulative NMEs with respect to the energies of  $1^+$  states of the intermediate nucleus for all three transitions. Our analyses reveal that the present shell-model

Hamiltonian partially describes the contribution of the GTGR region in the case of  $^{76}\text{Ge}$  for the  $0_{g.s.}^+ \rightarrow 0_{g.s.}^+$  transition, which was not obtained in the previous shell-model studies. Our calculations show single-state dominance (SSD) for the  $0_{g.s.}^+ \rightarrow 0_{g.s.}^+$  transition in  $^{96}\text{Zr}$ . The computed half-lives turned out to be in good agreement with the experimental data. Additionally, we compared the predicted NMEs with those obtained from different nuclear models in previous works. The shell-model predicted branching ratios for the  $2\nu\beta\beta$  decay of  $^{76}\text{Ge}$ , and both the single- $\beta$  and  $2\nu\beta\beta$  decay of  $^{96}\text{Zr}$  are also analyzed.

#### ACKNOWLEDGEMENTS

We acknowledge financial support from SERB (India), Grant No. CRG/2022/005167. Additionally, D.P. acknowledges financial support from MHRD, the Government of India. We would like to thank the National Supercomputing Mission (NSM) for providing computing resources of ‘‘PARAM Ganga’’ at the IIT Roorkee, implemented by C-DAC and supported by MeitY and DST, Government of India.

- 
- [1] F. F. Deppisch, L. Graf, and F. Šimkovic, Searching for New Physics in Two-Neutrino Double Beta Decay, *Phys. Rev. Lett.* **125**, 171801 (2020).
- [2] The GERDA Collaboration, Background-free search for neutrinoless double- $\beta$  decay of  $^{76}\text{Ge}$  with GERDA, *Nature* **544**, 47 (2017).
- [3] M. Agostini, A. Alexander, G. R. Araujo, A. M. Bakalyarov, M. Balata *et al.* (GERDA Collaboration), Final Results of GERDA on the Two-Neutrino Double- $\beta$  Decay Half-Life of  $^{76}\text{Ge}$ , *Phys. Rev. Lett.* **131**, 142501 (2023).
- [4] N. Ackerman, B. Aharmim, M. Auger, D. J. Auty, P. S. Barbeau *et al.* (EXO Collaboration), Observation of Two-Neutrino Double-Beta Decay in  $^{136}\text{Xe}$  with the EXO-200 Detector, *Phys. Rev. Lett.* **107**, 212501 (2011).
- [5] D. Q. Adams, C. Alduino, K. Alfonso, F. T. Avignone III, O. Azzolini *et al.*, Measurement of the  $2\nu\beta\beta$  Decay Half-Life of  $^{130}\text{Te}$  with CUORE, *Phys. Rev. Lett.* **126**, 171801 (2021).
- [6] S. R. Elliott, A. A. Hahn, and M. K. Moe, Direct evidence for two-neutrino double-beta decay in  $^{82}\text{Se}$ , *Phys. Rev. Lett.* **59**, 2020 (1987).
- [7] M. Goeppert-Mayer, Double Beta-Disintegration, *Phys. Rev.* **48**, 512 (1935).
- [8] R. Chandra, J. Singh, P. K. Rath, P. K. Raina, and J. G. Hirsch, Two-neutrino double- $\beta$  decay of  $94 \leq A \leq 110$  nuclei for the  $0^+ \rightarrow 0^+$  transition, *Eur. Phys. J. A* **23**, 223 (2005).
- [9] H. Ejiri, J. Suhonen, and K. Zuber, Neutrino-nuclear responses for astro-neutrinos, single beta decays and double beta decays, *Phys. Rep.* **797** 1, (2019).
- [10] T. R. Rodriguez and G. M.-Pinedo, Energy Density Functional Study of Nuclear Matrix Elements for Neutrinoless  $\beta\beta$  Decay, *Phys. Rev. Lett.* **105**, 252503 (2010).
- [11] N. Shimizu, J. Menéndez, and K. Yako, Double Gamow-Teller Transitions and its Relation to Neutrinoless  $\beta\beta$  Decay, *Phys. Rev. Lett.* **120**, 142502 (2018).
- [12] K. Zuber, Double beta decay, *Contemp. Phys.* **45**, 491 (2004).
- [13] R. Arnold, Augier, A. M. Bakalyarov, J. D. Baker, A. S. Barabash *et al.* (NEMO-3 Collaboration), Measurement of the double-beta decay half-life and search for the neutrinoless double-beta decay of  $^{48}\text{Ca}$  with the NEMO-3 detector, *Phys. Rev. D* **93**, 112008 (2016).
- [14] R. Arnold, C. Augier, A. S. Barabash, A. Basharina-Freshville, S. Blondel *et al.*, Final results on  $^{82}\text{Se}$  double beta decay to the ground state of  $^{82}\text{Kr}$  from the NEMO-3 experiment, *Eur. Phys. J. C* **78**, 821 (2018).
- [15] J. Argyriades, R. Arnold, C. Augier, J. Baker, A.S. Barabash, Measurement of the two neutrino double beta decay half-life of Zr-96 with the NEMO-3 detector, *Nucl. Phys. A* **847**, 168 (2010).
- [16] National Nuclear Data Center, Q-Value Calculator (QCalc), <https://www.nndc.bnl.gov/qcalc/>.
- [17] A. S. Barabash, Precise Half-Life Values for Two-Neutrino Double- $\beta$  Decay: 2020 Review, *Universe* **6**, 159 (2020).
- [18] E. Armengaud, C. Augier, A. S. Barabash, F. Bellini, G. Benato *et al.*, Precise measurement of  $2\nu\beta\beta$  decay of  $^{100}\text{Mo}$  with the CUPID-Mo detection technology, *Eur. Phys. J. C* **80**, 674 (2020).
- [19] A.S. Barabash, P. Belli, R. Bernabei, F. Cappella, V. Caracciolo *et al.*, Final results of the Aurora experiment to study  $2\beta$  decay of  $^{116}\text{Cd}$  with enriched  $^{116}\text{CdWO}_4$  crystal scintillators, *Phys. Rev. D* **98**, 092007 (2018).



- [20] A.P. Meshik, C.M. Hohenberg, O.V. Pravdivtseva, T.J. Bernatowicz, and Y.S. Kapusta,  $^{130}\text{Te}$  and  $^{128}\text{Te}$  double beta decay half-lives, *Nuclear Physics A* **809**, 275 (2008).
- [21] P. Novella, M. Sorel, A. Usón, C. Adams, H. Almazán *et al.* (NEXT Collaboration), Measurement of the  $^{136}\text{Xe}$  two-neutrino double- $\beta$ -decay half-life via direct background subtraction in NEXT, *Phys. Rev. C* **105**, 055501 (2022).
- [22] R. Arnold, C. Augier, J. D. Baker, A. S. Barabash, A. Basharina-Freshville *et al.* (NEMO-3 Collaboration), Measurement of the  $2\nu\beta\beta$  decay half-life of  $^{150}\text{Nd}$  and a search for  $0\nu\beta\beta$  decay processes with the full exposure from the NEMO-3 detector, *Phys. Rev. D* **94**, 072003 (2016).
- [23] J. Suhonen, and O. Civitarese, Probing the quenching of  $g_A$  by single and double beta decays, *Phys. Lett. B* **725**, 153 (2013).
- [24] J. Terasaki, and Y. Iwata, Estimation of nuclear matrix elements of double- $\beta$  decay from shell model and quasiparticle random-phase approximation, *Eur. Phys. J. Plus* **136**, 908 (2021).
- [25] J. Kostensalo, and J. Suhonen, Consistent large-scale shell-model analysis of the two-neutrino  $\beta\beta$  and single  $\beta$  branchings in  $^{48}\text{Ca}$  and  $^{96}\text{Zr}$ , *Phys. Lett. B* **802**, 135192 (2020).
- [26] M. Horoi, S. Stoica, and B. A. Brown, Shell-model calculations of two-neutrino double- $\beta$  decay rates of  $^{48}\text{Ca}$  with the GXPF1A interaction, *Phys. Rev. C* **75**, 034303 (2007).
- [27] D. Patel, P. C. Srivastava, V. K. B. Kota, and R. Sahu, Large-scale shell-model study of two-neutrino double beta decay of  $^{82}\text{Se}$ ,  $^{94}\text{Zr}$ ,  $^{108}\text{Cd}$ ,  $^{124}\text{Sn}$ ,  $^{128}\text{Te}$ ,  $^{130}\text{Te}$ ,  $^{136}\text{Xe}$ , and  $^{150}\text{Nd}$ , *Nucl. Phys. A* **1042**, 122808 (2024).
- [28] S. W. Finch, and W. Tornow, Search for two-neutrino double- $\beta$  decay of  $^{96}\text{Zr}$  to excited states of  $^{96}\text{Mo}$ , *Phys. Rev. C* **92**, 045501 (2015).
- [29] B. Pritychenko, Systematic analysis of double-beta decay half lives, *Nucl. Phys. A* **1033**, 122628 (2023).
- [30] A. Neacsu, and M. Horoi, An Effective Method to Accurately Calculate the Phase Space Factors for  $\beta^-\beta^-$  Decay, *Adv. High Energy Phys.* **2016**, 7486712 (2016).
- [31] S. Stoica, and M. Mirea, New calculations for phase space factors involved in double- $\beta$  decay, *Phys. Rev. C* **88**, 037303 (2013).
- [32] J. Kotila, J. Barea, and F. Iachello, Phase-space factors and half-life predictions for Majoron-emitting  $\beta^-\beta^-$  decay, *Phys. Rev. C* **91**, 064310 (2015).
- [33] J. Kotila, and F. Iachello, Phase-space factors for double- $\beta$  decay, *Phys. Rev. C* **85**, 034316 (2012).
- [34] J. T. Suhonen, Value of the Axial-Vector Coupling Strength in  $\beta$  and  $\beta\beta$  Decays: A Review, *Front. Phys.* **5**, 55 (2017).
- [35] T. Tomoda, Double beta decay, *Rep. Prog. Phys.* **54** 53 (1991).
- [36] J. Kostensalo, J. Suhonen, and K. Zuber, The first large-scale shell-model calculation of the two-neutrino double beta decay of  $^{76}\text{Ge}$  to the excited states in  $^{76}\text{Se}$ , *Phys. Lett. B* **831**, 137170 (2022).
- [37] M. Doi, T. Kotani, and E. Takasugi, Double Beta Decay and Majorana Neutrino, *Progress of Theoretical Physics Supplement* **83**, 1-175 (1985).
- [38] D. Patel, P. C. Srivastava, N. Shimizu, Systematic shell-model study of  $^{98-130}\text{Cd}$  isotopes and  $8^+$  isomeric states, *Nucl. Phys. A* **1039**, 122742 (2023).
- [39] A. Hosaka, K.-I. Kubo, and H. Toki,  $G$ -matrix effective interaction with the paris potential, *Nucl. Phys. A* **444**, 76 (1985).
- [40] X. Ji, and B. H. Wildenthal, Effective interaction for  $N = 50$  isotones, *Phys. Rev. C* **37**, 1256 (1988).
- [41] D. H. Gloeckner, Shell-model systematics of the zirconium and niobium isotopes, *Nucl. Phys. A* **253**, 301 (1975).
- [42] F. J. D. Serduke, R. D. Lawson, and D.H. Gloeckner, Shell-model study of the  $N = 49$  isotones, *Nucl. Phys. A* **256**, 45 (1976).
- [43] B.A. Brown, and W.D.M. Rae, The Shell-Model Code NuShellX@MSU, *Nucl. Data Sheets* **120**, 115 (2014).
- [44] N. Shimizu, T. Mizusaki, Y. Utsuno and Y. Tsunoda, Thick-restart block Lanczos method for large-scale shell-model calculations, *Comput. Phys. Comm.* **244**, 372 (2019).
- [45] NuDat 3 - National Nuclear Data Center, [https://www.nndc.bnl.gov/nudat3/indx\\_adopted.jsp](https://www.nndc.bnl.gov/nudat3/indx_adopted.jsp).
- [46] M. Honma, T. Otsuka, T. Mizusaki, Y. Utsuno, N. Shimizu, and M. Hjorth-Jensen, Shell-model description of magnetic dipole bands in  $^{105}\text{Sn}$ , *RIKEN Accel. Prog. Rep.* **51**, 95 (2018).
- [47] A. A. Klimenko, S. B. Osetrov, A. A. Smolnikov, and S. I. Vasiliev, Double-Beta Decay of  $^{150}\text{Nd}$  and  $^{76}\text{Ge}$  to Excited States, *Czechoslovak Journal of Physics* **52**, 589 (2002).
- [48] A. S. Barabash, A. V. Derbin, L. A. Popeko, and V. I. Umatov, Search for  $\beta\beta$  decay of  $^{76}\text{Ge}$  to the excited states in  $^{76}\text{Se}$ , *Z. Phys. A* **352**, 231 (1995).
- [49] C. Arpesella, A. S. Barabash, E. Bellotti, C. Brofferio, E. Fiorini *et al.*, Search for  $\beta\beta$  decay of  $^{96}\text{Zr}$  and  $^{150}\text{Nd}$  to excited states of  $^{96}\text{Mo}$  and  $^{150}\text{Sm}$ , *Europhys. Lett.* **27**, 29 (1994).
- [50] J. H. Thies, D. Frekers, T. Adachi, M. Dozono, H. Ejiri *et al.*, The  $(^3\text{He}, t)$  reaction on  $^{76}\text{Ge}$ , and the double- $\beta$ -decay matrix element, *Phys. Rev. C* **86**, 014304 (2012).
- [51] R. Arnold, C. Augier, J. Baker, A. Barabash, D. Blum *et al.*, Double beta decay of  $^{96}\text{Zr}$ , *Nucl. Phys. A* **658**, 299 (1999).
- [52] K. Nomura, Two-neutrino double- $\beta$  decay in the mapped interacting boson model, *Phys. Rev. C* **105**, 044301 (2022).
- [53] S. K. Dhiman and P. K. Raina, Two-neutrino double-beta decay matrix elements for ground and excited states of  $^{76}\text{Ge}$  and  $^{82}\text{Se}$  nuclei, *Phys. Rev. C* **50**, R2660(R) (1994).
- [54] J. Toivanen and J. Suhonen, Study of several double-beta-decaying nuclei using the renormalized proton-neutron quasiparticle random-phase approximation, *Phys. Rev. C* **55**, 2314 (1997).
- [55] L. Jokiniemi, B. Romeo, C. Brase, J. Kotila, P. Soriano, Two-neutrino  $\beta\beta$  decay of  $^{136}\text{Xe}$  to the first excited  $0^+$  state in  $^{136}\text{Ba}$ , *Phys. Lett. B* **838**, 137689 (2023).
- [56] F. Šimkovic, L. Pacearescu, and A. Faessler, Two-neutrino double beta decay of  $^{76}\text{Ge}$  within deformed QRPA, *Nucl. Phys. A* **733**, 321 (2004).
- [57] J. Kilgallon, M. R. Pearson, J. Billowes, P. Campbell, U. Georg *et al.*, Quadrupole moments and mean square charge radii in the bismuth isotope chain, *Phys. Lett. B* **405**, 31 (1997).
- [58] G. A. Lalazissis, S. Raman, and P. Ring, Ground-state properties of even-even nuclei in the relativistic mean-field theory, *At. Data Nucl. Data Tables* **71**, 1 (1999).

- [59] S. Stoica, Two-neutrino double-beta decay half-lives of  $^{96}\text{Zr}$  and  $^{100}\text{Mo}$  to excited states of  $^{96}\text{Mo}$  and  $^{100}\text{Ru}$ , *Phys. Lett. B* **350**, 152 (1995).
- [60] J. Suhonen and O. Civitarese, Weak-interaction and nuclear-structure aspects of nuclear double beta decay, *Phys. Rep.* **300**, 123 (1998).
- [61] J. Suhonen, *From Nucleons to Nucleus: Concepts of Microscopic Nuclear Theory*, Springer, Berlin, 2007.
- [62] M. Alanssari, D. Frekers, T. Eronen, L. Canete, J. Dilling *et al.*, Single and Double Beta-Decay  $Q$  Values among the Triplet  $^{96}\text{Zr}$ ,  $^{96}\text{Nb}$ , and  $^{96}\text{Mo}$ , *Phys. Rev. Lett.* **116**, 072501 (2016).
- [63] H. Heiskanen, M. T. Mustonen, and J. Suhonen, Theoretical half-life for beta decay of  $^{96}\text{Zr}$ , *J. Phys. G: Nucl. Part. Phys.* **34**, 837 (2007).